A. Degenève
Laboratoire EM2C,
CNRS, CentraleSupélec,
Université Paris-Saclay,
3, rue Joliot Curie,
Gif-sur-Yvette cedex 91192, France;
Air Liquide,
Centre de recherche Paris Saclay,
Chemin de la Porte des Loges,
B.P. 126,
Les Loges en Josas 78354, France

P. Jourdaine
Air Liquide,
Centre de recherche Paris Saclay,
Chemin de la Porte des Loges,
B.P. 126,
Les Loges en Josas 78354, France

C. Mirat
Laboratoire EM2C,
CNRS, CentraleSupélec,
Université Paris-Saclay,
3, rue Joliot Curie,
Gif-sur-Yvette cedex 91192, France

J. Caudal
Air Liquide,
Centre de recherche Paris Saclay,
Chemin de la Porte des Loges,
B.P. 126,
Les Loges en Josas 78354, France

R. Vicquelin
Laboratoire EM2C,
CNRS, CentraleSupélec,
Université Paris-Saclay,
3, rue Joliot Curie,
Gif-sur-Yvette cedex 91192, France

T. Schuller
Laboratoire EM2C,
CNRS, CentraleSupélec,
Université Paris-Saclay,
3, rue Joliot Curie,
Gif-sur-Yvette cedex 91192, France;
Institut de Mécanique des Fluides de Toulouse,
IMFT,
Université de Toulouse,
CNRS,
Toulouse 31400, France
e-mail: arthur.degeneve@centralesupelec.fr

Effects of a Diverging Cup on Swirl Number, Flow Pattern, and Topology of Premixed Flames

Impact of the diverging cup angle of a swirling injector on the flow pattern and stabilization of technically premixed flames is investigated both theoretically and experimentally with the help of OH chemiluminescence, OH laser-induced fluorescence and particle image velocimetry (PIV) measurements. Recirculation enhancement with a lower position of the internal recirculation zone (IRZ) and a flame leading edge protruding further upstream in the swirled flow are observed as the injector nozzle cup angle is increased. A theoretical analysis is carried out to examine whether this could be explained by changes of the swirl level as the diffuser cup angle is varied. It is shown that pressure effects need in this case to be taken into account in the swirl number definition and expressions for changes of the swirl level through a diffuser are derived. It is demonstrated that changes of the swirl level including or not the pressure contribution to the axial momentum flux are not at the origin of the changes observed of the flow and flame patterns in the experiments. The swirl number without the pressure term, designated as pressure-less swirl, is then determined experimentally with laser Doppler velocimetry (LDV) measurements at the injector outlet for a set of diffusers with increasing quarl angles under nonreacting conditions and the values found corroborate the predictions. It is finally shown that the decline of axial velocity and the rise of adverse axial pressure gradient, both due to the cross section area change through the diffuser cup, are the dominant effects that control the leading edge position of the IRZ of the swirled flow. This is used to develop a model for the displacement of the recirculation bubble as the quarl angle varies that shows very good agreement with experiments.* [DOI: 10.1115/1.4041518]

Introduction

Providing a rotational motion to the flow is widely used to ease flame stabilization in high power combustion systems. Despite extensive studies, see, for example, the pioneering work in Ref. [1], the stabilization mechanisms of swirled flames are still the topic of many recent investigations due to their complex structure and dynamics [2].

The structure of a swirling flame is known to depend largely on the structure of the irrotational jet exhausting the injector [3–6]. The swirl number [3,4], the inlet geometry of the injector [7,8] and the flow confinement [9,10] are the main parameters affecting the flame topology. Heat losses to the chamber walls are also known to alter the structure of the reacting flow [11,12]. A central bluff-body [2,13,14] and a diffuser [2,4,13,15–17] constitute other widely used elements to enhance the stabilization of swirling flames. In high power systems, it is, however, more suitable to operate without any central insert to reduce the thermal stress on the solid components of the injector.

The diverging cup of the injector nozzle, also designated by quarl or diffuser, drastically changes the topology of the flow so as to favor flame stabilization inside the internal recirculation zone (IRZ). Gupta and Lilley [4] and Vanoverberghe et al. [15] investigated the combination of swirl, quarl, and bluff-body to identify and classify the different flow patterns observed under nonreacting flow conditions. Increasing the quarl angle enhances the mass flow rate in the IRZ [15,18], increases its size and lowers its position along the burner axis [4,13] improving flame stabilization. Adding a quarl is often used to improve the operability of a burner over a wider range of flow operating conditions. However, as already noticed in Ref. [15], there are still yet a limited number of studies on effects of the quarl for aerodynamically swirl-stabilized flames in setups without bluff-body.

Both quarl and swirl separately provide interesting features to the resulting flow, yet adding a quarl to a swirling injector may alter the value of the swirl level due to changes of the velocity profiles in the diffuser. Chigier and Beér [13] introduced the swirl number $S = G_\theta/(\mathrm{R}G_z)$ to characterize the level of swirl of the flow, where $G_\theta = \int_A \rho r u_\theta u_z \mathrm{d}A$ is the axial flux of tangential momentum, $G_z = \int_A (\rho u_z^2 + (p - p_\infty))\mathrm{d}A$ the axial momentum flux, and R a characteristic dimension of the injector.

Gupta and Lilley [4] have theorized the impact of a change of cross section on the value of the swirl number. As in the majority of the works [19], they assume the pressure term in G_z to be negligible. This approximation leads to the definition of a pressure-less swirl number $\widetilde{S}$ calculated with $\widetilde{G}_z = \int_A \rho u_z^2 \mathrm{d}A$. Assuming simplified velocity profiles, they model the impact of a quarl on the swirl number as

$$\frac{\widetilde{S}_2}{\widetilde{S}_1} = \frac{R_2}{R_1} \tag{1}$$

where R_1 and R_2 are the radius of the diffuser cup inlet and outlet cross sections. Experiments presented in this work show that Eq. (1) cannot be a substitute for the complex velocity profiles issuing from a swirling injector. This has motivated further investigation. Change of the swirl level through a change of the cross section area of the flow passage is here revisited both theoretically and experimentally.

Measuring the swirl number S raises experimental difficulties. As reported in many studies, swirling flows of practical interest are highly turbulent [19], and Reynolds averages of the axial and azimuthal momentum fluxes lead to new contributions associated with turbulent fluctuations $\overline{G_{z_t}} = \int_A (\rho(\overline{u_z}^2 + \overline{u_z'^2}) + (\overline{p} - p_\infty))\mathrm{d}A$ and $\overline{G_{\theta_t}} = \int_A \rho r(\overline{u_\theta}\,\overline{u_z} + \overline{u_\theta' u_z'})\mathrm{d}A$. In the outer regions of the swirling jet, the mean velocities $\overline{u}_z$ and $\overline{u}_\theta$ drop to zero whereas the turbulent components $\overline{u'^2}_z$ and $\overline{u_z' u'}_\theta$ due to the recirculating flow pattern remain significant. Similarly, $\overline{p} - p_\infty$ is large when compared to $\rho\overline{u_z}^2$ in the outer region of the jets. Hence, measuring $\overline{G_{z_t}}$ and $\overline{G_{\theta_t}}$ in a turbulent swirling flow requires to probe the velocity field up to the vicinity of the walls where the turbulent and pressure terms are weighted by r^2 to estimate these integrals.

Some authors [4,20] suggest to integrate by part the axial momentum flux, which brings out the static pressure on the wall. Thanks to wall pressure measurements, Mattingly et al. [20] verified the conservation of axial momentum flux G_z in a tube of constant cross section area. Other authors directly measured the radial distribution of static pressure within the flow with the help of Pitot probes [4,20]. Chigier and Beér [13] and Mahmud et al. [21] found that both G_z and G_θ momentum fluxes remain constant within a straight tube provided effects of pressure are included in the momentum flux G_z. However, Pitot probes are intrusive devices and smooth out turbulent fluctuations.

These previous investigations show that measuring the swirl number is a difficult task due to the contributions from pressure and turbulent fluctuations. For a flow in a duct with a smooth cross section area change over a short distance with respect to the duct diameter, effects of turbulence can be discarded as a first approximation because changes of the flow pattern are essentially controlled by an inviscid process. A theoretical analysis is carried out in this work to estimate the contribution from the pressure term in the swirl level due to changes of the cross section area through an injector. This problem constitutes the first objective of this paper.

The second objective is to understand how the flow structure and flame stabilization are altered when the angle of the diffuser cup of the injector is modified. An experimental analysis is conducted to isolate effects of the quarl angle, all other parameters remaining fixed. It is shown that measurements of the pressure-less swirl number do not obey to Eq. (1), and this has motivated a further theoretical investigation of the swirl number evolution through a diffuser with the introduction of shape factors. It is finally shown that independently of the definition of the swirl number, changes of the swirl level cannot be used to explain the changes of the average reacting and nonreacting flow fields observed in the experiments when the injector diffuser cup angle widens. This in turn has led to the development of a new model for the evolution of the leading edge position of the internal recirculation zone of a swirling injector when the quarl angle is varied.

The paper is organized as follows: The experimental setup is described in first, followed by an analysis of the flame and flow structures in reacting conditions for varying quarl angles. Measurements of swirl number on a pressure-less basis are then carried out under-nonreacting conditions. Theory is then pushed forward to include pressure effects and examine the impact of a smooth change of the cross section area of the injector on the swirl number. Finally, a model is developed to account for the displacement of the position of the IRZ in the combustion chamber when the diverging cup angle is modified.

Experimental Setup

The test rig and the optical diagnostics are the same as those used to investigate effects of swirl on the stabilization of technically premixed methane/air flames in a configuration where the injection nozzle is equipped with a diverging cup angle $\alpha = 10$ deg [17]. This setup was also used to compare the stabilization of CO_2- and N_2-diluted oxy-methane flames and examine scaling

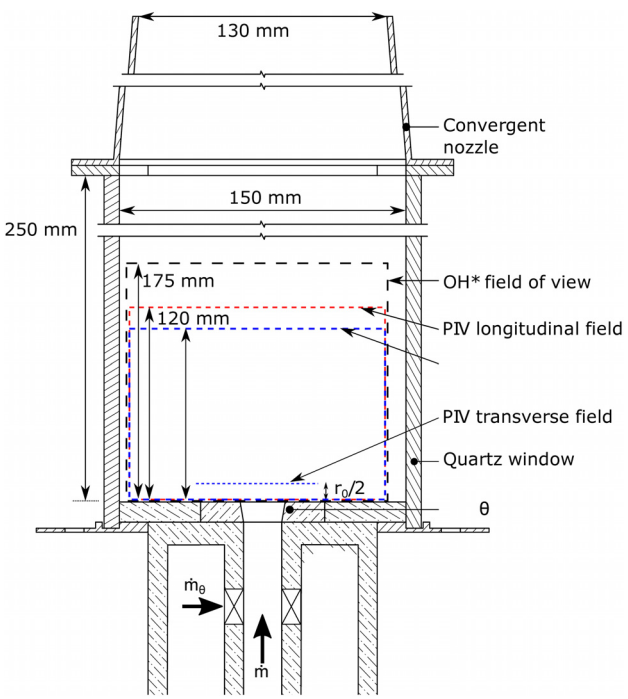

Fig. 1 OXYTEC atmospheric test-rig

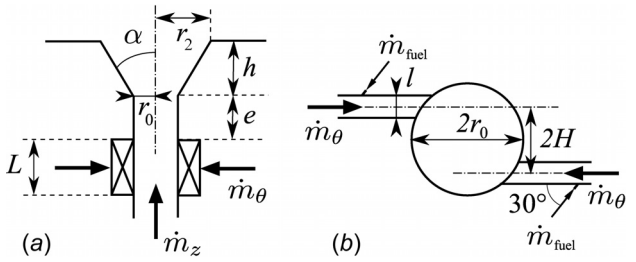

Fig. 2 Sketch of the injector: (*a*) axial cut and (*b*) transverse cut through the swirler

rules when switching from air- to oxy-combustion operating mode with the same injector [17,22]. Only the main elements of the test rig are briefly described below. The reader is referred to Refs. [17], [22], and [23] for more details.

Figure 1 shows a schematic of the Oxytec combustor. The combustion chamber has a square cross section of 150 mm width and 250 mm length. Four quartz windows provide a large optical access to the combustion region. The burnt gases are exhausted to the atmosphere at ambient pressure through a nozzle with an area contraction ratio of 0.8. The combustion chamber dump plane in contact with the burnt gases is cooled by water circulation. Its temperature is kept constant and equal to $T_p = 450$ K during all experiments.

Methane and air are mixed within a swirling injector sketched in Fig. 2. The swirling motion is produced by an axial-plus-tangential entry swirl generator where $\dot{m}_\theta$ and $\dot{m}_z$ are the mass flowrates injected tangentially and axially. Assuming an uniform axial flow profile and a solid body rotation for the azimuthal velocity, a geometrical swirl number S_0 can be defined at the injector outlet [4]

$$S_0 = \frac{\pi}{2}\frac{Hr_0}{NlL}\frac{1}{1+\dot{m}_z/\dot{m}_\theta} \tag{2}$$

where H is the distance separating the tangential injection channels from the burner axis, r_0 is the injector radius, and l and L are the width and the height of the N tangential injection channels. This device was designed to produce geometrical swirl numbers ranging from $S_0 = 0$–1.75 with $N = 2$ slits. More details on the fuel injection system are given in Ref. [23].

The methane/air mixture leaves the swirler through a $r_0 = 10$ mm cylindrical channel and flows into the combustion chamber through an end piece equipped with a diffuser with a variable cup angle α. The height of the diffuser cup is $h = 10$ mm. Partially premixed conditions are achieved at the injector outlet at $z/r_0 = 0$ [17] and fully premixed conditions were confirmed by large eddy simulations at $z/r_0 = 0.5$ in a region where the flame leading edge is stabilized for most operating conditions [23].

Care was taken to wait for thermal equilibrium of the chamber solid components before making measurements [24]. OH* chemiluminescence images are used to investigate the mean structure taken by the flames. OH planar laser-induced fluorescence (OH-PLIF) snapshots are used to determine the probability of presence of the flame front in the axial plane of the test-rig. A set of 1500 images is taken to deduce the probability of presence of the hot burnt gases. The gradient of these images is then used to detect the flame front between the fresh gases and the hot burnt gases. Averages of these images yield the probability of presence of the flame front. A series of tests were made to check the statistical convergence of the data and the sensitivity of the results to the threshold level used to detect the flame front. The reader is referred to Ref. [23] for more details on the postprocessing.

These experiments are completed by particle image velocimetry (PIV) measurements in cold and hot flow conditions in the axial and different transverse planes above the injector. PIV and OH-PLIF are here combined to reveal the mean structure taken by the flow and flame produced by the axial-plus-tangential swirler. Two component laser Doppler velocimetry (LDV) measurements are used to determine the axial and tangential velocity components of the nonreacting swirling flow at the injector outlet. These data are used to determine the (pressure-less) swirl number. The diagnostics, the tests made, and the different postprocessing techniques are fully described in Refs. [17] and [23].

All experiments presented in this work are conducted at the equivalence ratio $\phi = 0.95$ for a thermal power $P = 13$ kW corresponding to a Reynolds number Re = 18,000 based on the injection tube diameter $2r_0 = 20$ mm and the bulk temperature $T_u = 293$ K. The geometrical swirl number calculated with Eq. (2) is also kept constant and equal to $S_0 = 0.85$. Note that effects of the diverging cup are not taken into account in this definition of the swirl number.

Flame and Flow Structures

Before examining the flame structure, it is worth attempting an analysis of the main parameters controlling the flame shape. The height of the combustion chamber being fixed, the main important parameters identified in the scientific literature are the injection Reynolds number Re [25], the quarl angle α [15,18], the swirl number S [3,4], and the confinement ratio $C_r = W^2/(\pi r_2^2)$ [9,10], where $W = 150$ mm is the width of the combustion chamber, and r_2 is the nozzle radius at the diffuser cup outlet. The quarl angle varies in studies from $\alpha = 0$ to 45 deg leading to changes of the confinement ratio $18 \leq C_r \leq 72$. As a consequence, the injector of the Oxytec test-rig operates according to Ref. [9] in the free-jet regime for all quarl angles tested. This regime is typical of a swirling jet exhausting into unconfined atmosphere and of confined systems with sidewalls aways from the injector nozzle [24].

Figure 3 shows the distribution of the OH* spontaneous light emission for different quarl angles α, all other geometrical and flow parameters remaining constant. With a straight injector, $\alpha = 0$ deg, the flame is lifted and takes a V-shape above the burner with a flame leading edge far from the burner exit despite the large swirl level $S_0 = 0.85$ imparted to the flow. As α increases from 5 deg to 30 deg, the flame widens in the transverse direction, shrinks in the axial direction and its leading edge moves further upstream toward the injector. For larger values $\alpha \geq 45$ deg, the

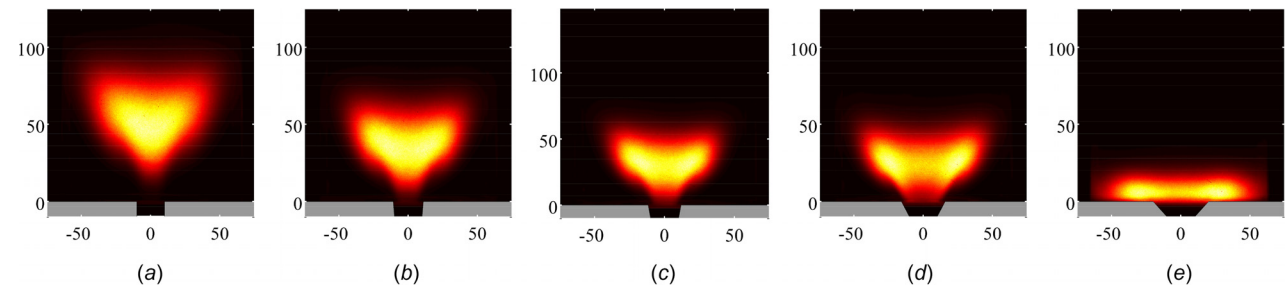

Fig. 3 OH* intensity distribution as a function the diverging cup angle α. Gray elements indicate solid components of the combustor. Dimensions are in millimeters: (*a*) $\alpha = 0$ deg, (*b*) $\alpha = 5$ deg, (*c*) $\alpha = 10$ deg, (*d*) $\alpha = 30$ deg, and (*e*) $\alpha = 45$ deg.

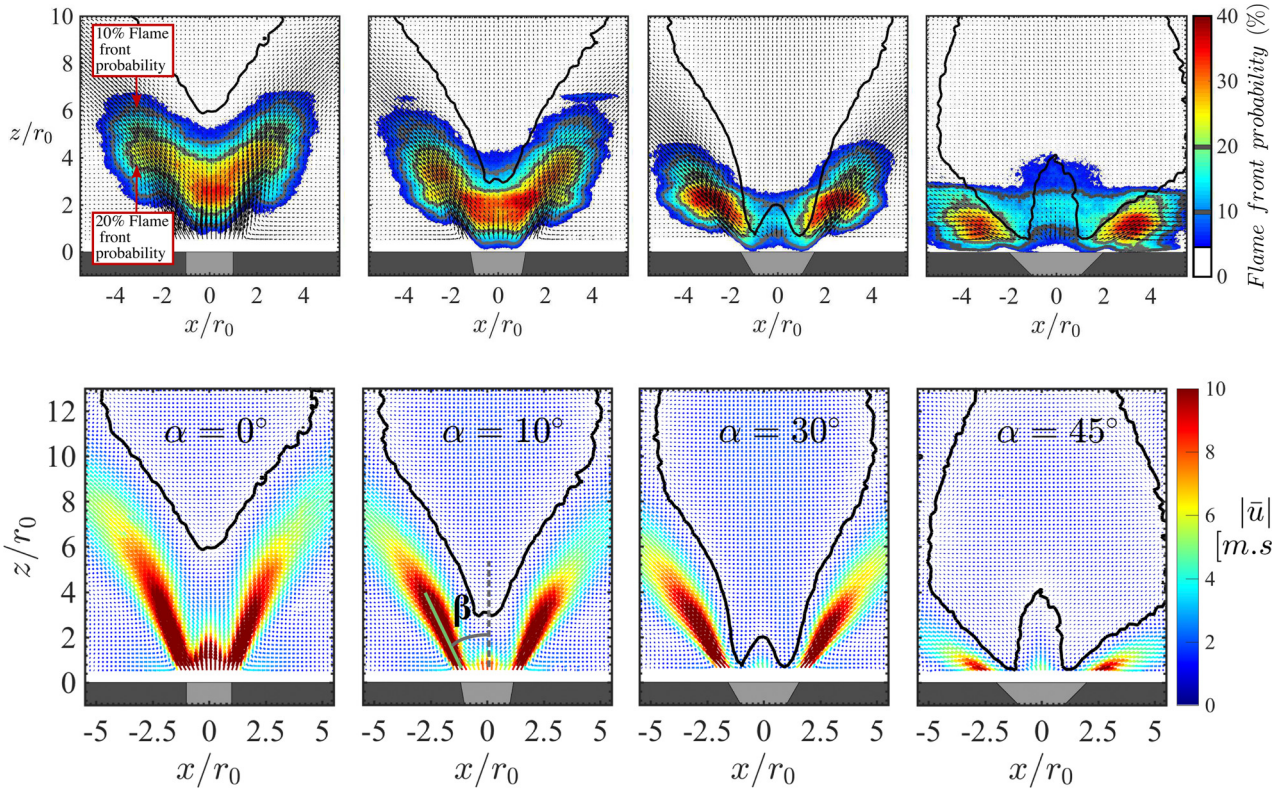

Fig. 4 Top: probability of presence of the flame front deduced from OH-PLIF measurements in an axial plane with the overlaid velocity field. The gray lines delineate the positions where the flame front is present 20% and 10% of the time. Bottom: velocity field colored by the velocity magnitude $|\overline{u}| = (\overline{u}_z^2 + \overline{u}_x^2)^{1/2}$ obtained by PIV. The black contour delineates the position of the IRZ where the axial velocity $\overline{u}_z$ is zero.

flame suddenly flattens, and the combustion reaction takes place in the boundary layer close to the combustor dump plane. The flame takes in these cases a torus shape in the so-called wall jet regime [4,13], also referred as Coanda stabilized flame [15].

The same experiments were repeated at a lower swirl number $S_0 = 0.75$ in Ref. [26], wherein a more detailed study is carried out on the influence of the swirl level on the flame topology. The same observations were made. Increasing the quarl angle moves the flame leading edge upstream, reducing the flame length and widening its shape in the radial direction. These observations are common to many studies conducted with different types of swirling injectors in premixed and nonpremixed combustion modes with gaseous or liquid fuel injections [4,15].

Further analysis is carried out by examining the structure of the flow field and flame in an axial plane. Figure 4 shows on the top the probability of presence of the flame front superimposed to the velocity field obtained by PIV in reacting conditions for different diffuser cup angles, all other parameters remaining fixed. The gray countors represent the position where the flame front is present 20% (inner contour) and 10% (outer contour) of the time. The position of the IRZ is represented by the black contour. The position of the outer recirculation zones (ORZ) is not reproduced in this figure. The bottom images show the same velocity fields on a slightly zoomed field of view together with the magnitude $|\overline{v}| = (\overline{u}_z^2 + \overline{u}_x^2)^{1/2}$ of the velocity vectors $\overline{\mathbf{v}} = \overline{u}_z \mathbf{e}_z + \overline{u}_x \mathbf{e}_x$ represented by the colored scale. The black line delineates the position where the axial velocity $\overline{u}_z = 0$ is null, delimiting the boundary of the IRZ. The contours of zero axial velocity delineating the ORZ are not represented here.

For a straight injection nozzle $\alpha = 0$ deg, the V-shaped flame features a leading edge front located along the burner axis at a distance $z_f/r_0 = 1.8$ above the injector outlet, identified here as a probability of presence of the flame front equal to $p = 20\%$. The stagnation point corresponding to the leading edge of the IRZ $z_{SP}/r_0 = 5.9$ is also located along the burner axis and lies far away from the flame. Note also that the maximum probability of presence of the flame front does not exceed in this case $p < 30\%$ in Fig. 4 ($\alpha = 0$ deg) highlighting the strong intermittency of the combustion process, a characteristic of turbulent swirling flames stabilized far away from the injector outlet. It can be noticed that the combustion reaction takes also place between the ORZ and the outer swirling jet shear layer. The flame takes in this case intermittently an M-shape, with rapid transitions back to its V-shape. The probability of presence of the M-shape structure remains small $p < 20\%$ due to large cross section area change at the injector outlet of the combustor leading to high thermal losses in the ORZ [12]. The ORZ is too cold to sustain combustion between the ORZ and the outer shear layer of the swirling jet.

When the injection nozzle is equipped with a diffuser cup angle $\alpha = 10$ deg, the flame still mainly features a V-shape in Fig. 4 ($\alpha = 10$ deg), but lies closer to the injector outlet with a leading edge front at $z_f/r_0 = 1.0$. The probability of presence of the flame front increases above $p \geq 20\%$ in the combustion chamber with a large region with $p \sim 35\%$. The maximum probability of presence of the flame leading edge front now lies on both sides of the burner axis, above the regions featuring the lowest axial velocities at $|x|/r_0 = 0.8$. This is due to the peculiar structure of the jet flow at the nozzle outlet produced by this axial-plus-tangential injector. The flame leading edge preferentially lies in a region comprised between the burner axis where the axial velocity reaches a local maximum and the inner shear layer of the swirling jet at $|x|/r_0 = 1.2$ where the velocities are the highest. The trace of the statistical distribution of the leading edge reaction layer follows the axial velocity profile and takes a smoothed but discernable W-shape. One may also note that the leading edge of the IRZ lying at the altitude $z_{SP}/r_0 = 3.0$ is no longer located along the burner axis.

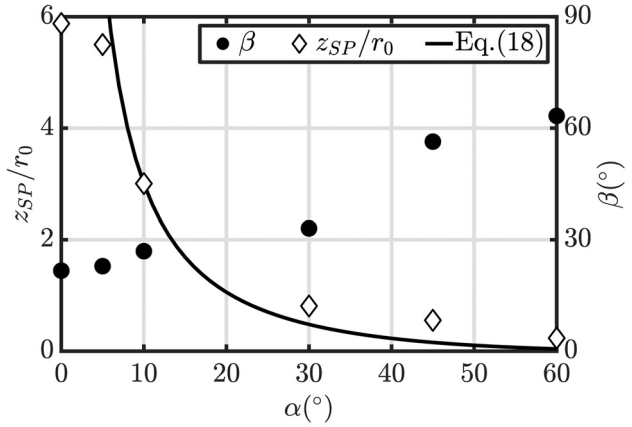

Fig. 5 Angle β (black disks) of the swirling jet flow at the injector outlet and position of the IRZ leading edge stagnation point z_{SP}/r_0 measured (empty diamonds) and predicted by Eq. (18) (continuous line) as function of the diffuser cup angle α

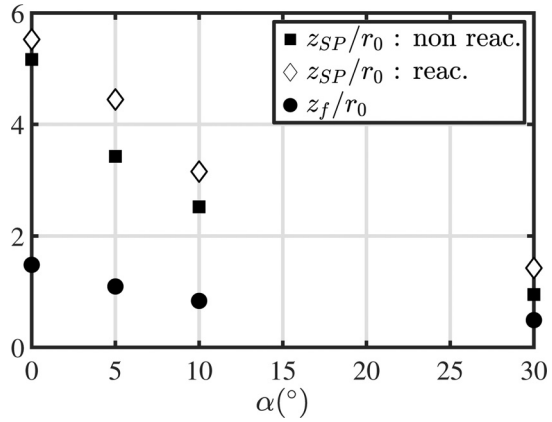

Fig. 6 Internal recirculation zone leading edge position z_{SP}/r_0 in nonreacting (black squares) and reacting (empty diamonds) flow conditions, and flame leading edge position z_f (black disks) as a function of the injector diffuser cup angle α

The flame front probability of presence at the interface between the ORZ and the outer shear layer of the swirling jet has slightly increased with values $p > 20\%$, meaning that the probability to find an M-shaped flame structure has slightly increased compared to injection with the straight injection tube ($\alpha = 0$ deg).

When the diffuser cup angle is further increased to $\alpha = 30$ deg, the flame now switches intermittently between a V-shape and an M-shape with about the same probability. The position of the IRZ leading edge moves very close to the maximum probability of presence of the flame front at $z_{SP}/r_0 = 0.8$ and is off-axis by $|x|/r_0 = 1.0$ in Fig. 4 ($\alpha = 30$ deg). Note that the stagnation point of the IRZ along the burner axis lies much further away at $z_{SP}/r_0 = 1.8$. The flame leading edge position also lies off-axis at the same distance $z_f/r_0 = 0.8$ as the leading edge of the IRZ, but is pushed radially away from the burner axis at $|x|/r_0 = 1.5$. The main difference with results for a cup angle $\alpha = 10$ deg is that for $\alpha = 30$ deg the IRZ now protrudes far upstream within the swirled flow and lies close to the injector outlet. This protruding IRZ shrinks the size of the flame in the axial direction with almost no reaction left in the central region of the flow and pushes the combustion zone toward the side of the burner. The probability of presence of the flame front remains lower than $p < 15\%$ along the burner axis. The combustion reaction is now essentially concentrated in the internal and external shear layers of the flow between the IRZ and ORZ. On average the trace of the distribution of the leading edge of the flame reaction layer lies again in the zones of low axial velocities at $|x|/r_0 = 1.0$ and takes a W-shape. This W-shape is now more apparent than for the case with $\alpha = 10$ deg.

For a diffuser cup angle $\alpha = 45$ deg, the flame takes a torus shape stabilized close to the dump plane of the injector in a wall jet regime in Fig. 4 ($\alpha = 45$ deg). This flow regime is characterized by the disappearance of the ORZ and a predominant IRZ bubble occupying almost all the combustion chamber except the central region of the flow close to the injector outlet. The probability of presence of the flame front increases now up to values $p \sim 40\%$ and the reaction mainly takes place along the arms of the swirling jet. In this wall jet regime, the IRZ does not move further upstream, but grows bigger in the transverse direction, because the axial velocity at the burner outlet is high enough to avoid flashback. This feature is a specificity of the axial-plus-tangential swirler used in this study allowing independent control of the axial and tangential mass flowrates injected in the burner and is used to prevent flashback [17,27].

Effects of the quarl angle are further analyzed by measuring the jet opening angle β of the swirling jet. This angle represented in the second image at the bottom in Fig. 4 ($\alpha = 10$ deg) is defined as the angle between the vertical axis and the line of maximum velocity reached by the jet flow over the first 10 mm above the injector outlet. The evolution of β is plotted in Fig. 5 as a function of the diffuser cup angle α. The position of the stagnation point z_{SP} defined as the lowest axial position of the IRZ is also represented in this figure. The angle β linearly increases with α below $\alpha \leq 30$ deg. It then changes abruptly for $30\,\text{deg} < \alpha < 45\,\text{deg}$ when the jet switches from the free jet to the wall jet regime. This analysis confirms that the swirling jet angle β regularly increases like the angle α of the diffuser cup as long as the swirling jet flow lies in the free jet regime.

The flow field is now analyzed by comparing measurements in reacting and nonreacting conditions. PIV data gathered under nonreacting conditions are not shown here (see Ref. [17]). In these experiments, the bulk flow velocity is compensated for the absence of fuel in the nonreacting conditions. Figure 6 represents the IRZ leading edge position z_{SP}/r_0 in reacting (black squares) and nonreacting (empty diamonds) conditions. The position of the flame leading edge front z_f/r_0 (black disks) is also plotted. The combustion reaction slightly alters the position of the IRZ. Acceleration of the burnt gases due to thermal expansion pushes the IRZ a bit further downstream from the injector outlet, but differences for z_{SP}/r_0 between cold flow and hot flow results remain small. This figure also confirms that the flame leading edge z_f/r_0 always lies upstream the IRZ leading edge z_{SP}/r_0 with and without the combustion reaction. Consequently, measurements of the flow in nonreacting conditions allow to infer the position of the leading point of the IRZ and the flow regime of the swirling jet in reacting conditions with good confidence.

Swirl Number Measurements

Laser Doppler velocimetry measurements are carried out in nonreacting conditions to determine the three components of the velocity field at the injector outlet. In these experiments, the bulk flow velocity in the injector is compensated for the absence of fuel. The results for the mean (a)–(b) and rms (c)–(d) velocities are presented in Fig. 7 for quarl angles $0\,\text{deg} \leq \alpha \leq 30\,\text{deg}$. As the pressure field could not be determined, the axial momentum G_z is approached by its pressure-less equivalent $\widetilde{G_z}$, yielding the pressure-less swirl number $\widetilde{S}$

$$\widetilde{S} = \frac{\int_A r\overline{u}_z\overline{u}_\theta \mathrm{d}A}{r_2\int_A \overline{u}_z^2 \mathrm{d}A} \tag{3}$$

where r_2 is the diffuser outlet radius, and A denotes the integration area over the entire cross section of the combustion chamber.

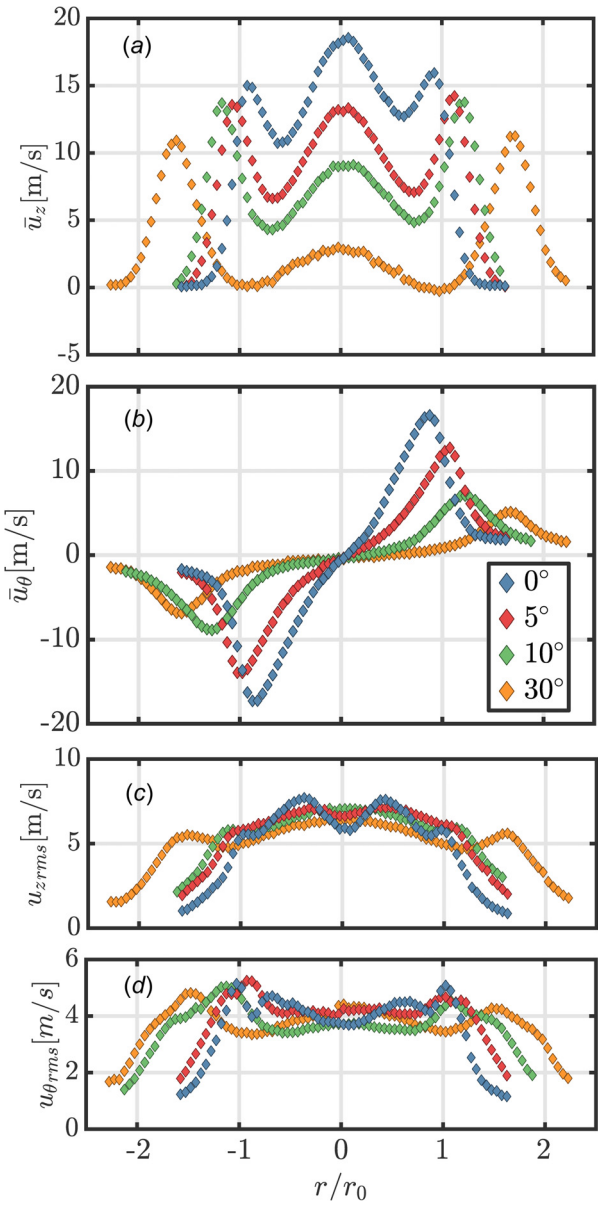

Fig. 7 Laser Doppler velocimetry measurements of the cold swirling flow for $\alpha = 0$, 5, 10, and 30 deg. $S_0 = 0.85$, Re = 18,000: (*a*) mean axial velocity, (*b*) mean azimuthal velocity,(*c*) rms axial velocity fluctuation, and (*d*) rms azimuthal velocity fluctuation.

As both $\overline{u}_z$ and $\overline{u}_\theta$ drop to zero out of the swirling jet, it has been verified that the measured value for $\widetilde{S}$ does not depend on the choice of the size of the integration area A. When measured at $z/r_0 = 0.5$, the axial and tangential velocities are always null at the end of the probed volume. These conditions could not be met further downstream $z/r_0 > 0.5$ or for large quarl angles $\alpha \geq 45$ deg due to the limited optical access through the combustion chamber.

One reminds that the geometrical swirl number $S_0 = 0.85$ is kept constant for all explored cases. It was not possible to perform exploitable measurements of the swirl number in the wall jet regime for $\alpha = 45$ deg. The measured values for $\widetilde{S}$ are reported in Table 1 for $\alpha = 0$, 10, and 30 deg. It is found that the swirl number $\widetilde{S}$ remains roughly unaltered when the diverging cup angle is varied between $0 \leq \alpha \leq 30$ deg with the axial-plus-tangential swirler used in this study

$$\widetilde{S}_{R_2}/\widetilde{S}_{R_1} \simeq 1 \tag{4}$$

Table 1 Measured swirl numbers $\widetilde{S}$ for Re = 18,000 and velocity profiles at $z/r_0 = 0.5$ for different quarl angles α

α (deg)	0	5	10	30
$\widetilde{S}$	0.78	0.72	0.78	0.74

where R_2 and R_1 stand for the outlet radius r_2 of two different diffusers. This result is at variance with the simplified model Eq. (1) from Gupta and Lilley [4] yielding an increasing swirl level as the quarl angle α increases.

It has been shown on the same setup in Ref. [17] that increasing the swirl level, with a swirl number measured on a pressure-less basis, shortens the flame and shifts the central recirculation zone further upstream. Figures 3 and 4 revealed that enlarging the quarl angle α from 0 deg to 30 deg lowers the position of the IRZ with a flame leading edge protruding further upstream within the swirled flow, but the pressure-less swirl number $\widetilde{S}$ at the injector outlet remains however unaltered. At this point, either the common assumptions made to measure the swirl number are inadequate to configurations featuring a diverging quarl or the swirl number is not the relevant quantity to investigate the behavior of an injector when the diffuseur cup angle is modified.

One may first wonder if this difference could be attributed to effects of turbulence that would alter the swirl level between the inlet and outlet of the diffuser cup. As mentioned previously, the rms velocity fluctuations plotted in Figs. 7(*c*) and 7(*d*) do not drop to zero away from the burner axis and these data cannot be used to make reliable estimates of the swirl number. However, it appears that the turbulence level is high for the four flows produced by the different quarls. With the $\alpha = 30$ deg quarl, the rms velocities even surpass the mean values over a large section of the combustion chamber. Finally, the rms values reached by the axial and azimuthal velocities barely change in Figs. 7(*c*) and 7(*d*) when the quarl angle varies from $\alpha = 0$ to 30 deg. One can, therefore, hypothesize that taking into account the contributions from the turbulent velocity fluctuations in the swirl number estimates would also lead to reduced variations of the swirl number when the quarl angle is varied.

As stated in the introduction, the experiments from Chigier and Beér [13] and Mahmud et al. [21] show that the momentum fluxes G_θ and G_z remain constant when the static pressure is included in the calculation of G_z. A theoretical analysis is developed in the following to shed further light on this issue.

Theoretical Analysis

The analysis is made by starting from first principles for a constant density flow. As sketched in Fig. 8, a fixed control volume is considered with a cross section inlet A_1 and a cross section outlet A_2 oriented along the vertical axis $\mathbf{e}_z$. This volume is bounded on its lateral side by an impermeable boundary over a surface area Σ Rotational symmetry of the flow and of the control volume boundaries are assumed. For a steady, inviscid, turbulence free, and gravity free flow, projection of the axial and azimutal momentum balances along the vertical axis yields

$$\begin{cases} \displaystyle\int_{A_2} (\rho u_z^2 + p)\mathrm{d}A - \int_{A_1} (\rho u_z^2 + p)\mathrm{d}A = -\int_\Sigma p\mathbf{n}\cdot\mathbf{e}_z\mathrm{d}A \\ \displaystyle\int_{A_2} \rho r u_\theta u_z \mathrm{d}A - \int_{A_1} \rho r u_\theta\, u_z \mathrm{d}A = 0 \end{cases} \tag{5}$$

where $\mathbf{n}$ is the external normal unit vector to the control volume boundary.

The quantity $p_\infty \int_A \mathbf{n}\cdot\mathbf{e}_z \mathrm{d}A = 0$ is subtracted from the momentum balance, where p_∞ corresponds to the ambiant pressure, which is taken constant. One is left with

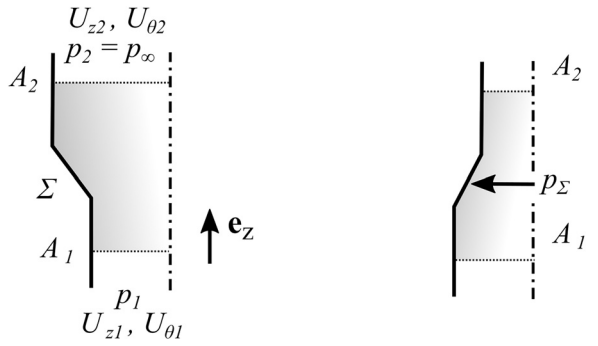

Fig. 8 Model for the theoretical analysis. Right: the swirl number increases in a converging nozzle because $p_\Sigma > p_\infty$ ($C_F < 0$). Left: the swirl number decreases in a diffuser because $p_\Sigma < p_\infty$ ($C_F > 0$) provided the pressure loss is not too large.

$$\begin{cases} G_{z2} - G_{z1} = F_z \\ G_{\theta 2} - G_{\theta 1} = 0 \end{cases} \tag{6}$$

where G_{zj} and $G_{\theta j}$ are, respectively, the axial and tangential momentum flux projections through the cross sections A_j with $j = 1, 2$

$$G_{zj} = \int_{A_j} (\rho u_z^2 + (p - p_\infty))\mathrm{d}A, \quad G_{\theta j} = \int_{A_j} \rho r u_\theta u_z \mathrm{d}A \tag{7}$$

and F_z denotes the axial force exerted by the solid boundaries on the flow. Due to the rotational symmetry, this force is oriented along the vertical axis

$$F_z = -\int_\Sigma (p - p_\infty)\mathbf{n} \cdot \mathbf{e}_z \mathrm{d}A \tag{8}$$

The choice of p_∞, albeit indisputable for an unconfined jet exhausting in quiescent air, can be debated when the jet flows into a combustion chamber, where the mean pressure differs from atmospheric pressure. In this theoretical study, confinement is not taken into account, so that the pressure at the diffuser outlet corresponds to $p_2 = p_\infty$.

One designates by $C_F = F_z/G_{z1}$ the force F_z made dimensionless by the axial momentum flux in section 1. The swirl number is also defined as $S = G_\theta/(RG_z)$, where R is the radius of the cross section area of interest. The evolution of the swirl number S between an inlet with section A_1 and and outlet with section A_2 can thus be expressed as

$$\frac{S_2}{S_1} = \frac{R_1}{R_2}\frac{1}{1 + C_F} \tag{9}$$

Assuming that the two axial momentum fluxes are positive quantities, $G_{z1} \geq 0$ and $G_{z2} \geq 0$, Eq. (6) yields the folllowing inequality for C_F: $-1 \leq C_F \leq G_{z2}/G_{z1}$. The evolution of the swirl number through a tube with a variable cross section area is controlled by the pressure force applied to the side wall in the axial direction through the ratio $C_F = F_z/G_{z1}$ in Eq. (9). Since the azimuthal momentum G_θ remains unaltered for an inviscid flow along a duct, the swirl variation is driven by the rate of conversion of the initial axial momentum flux G_{z1} to the axial force F_z exerted on the side wall.

Let consider the generic cases of a nozzle and a diffuser as sketched in Fig. 8. Equation (9) shows that the swirl number necessarily increases in the converging nozzle because $p_\Sigma > p_\infty$ and the ratio C_F is negative. It results in an increase of the swirl number due both to $R_1/R_2 > 1$ and $(1 + C_F)^{-1} > 1$.

The case of the diverging cup shown on the right in Fig. 8 is more difficult to handle and does not lead to a systematic conclusion. The pressure distribution along the lateral wall now depends on the eventual presence of recirculation zones due to flow separation inside the diffuser. This pressure distribution is in this case much more sensitive to the exact geometry of the diffuser [28]. The pressure drop through the device results from a competition between the conversion of kinetic energy and pressure losses modeled here by a singular pressure loss coefficient k. In typical air swirling injectors, the head loss remains generally weak, and one seeks to keep C_F as low as possible to limit pressure losses. This leads in Fig. 8 to a decrease in the swirl number between the inlet and the outlet cross sections of a diverging cup. The sign of C_F in Fig. 8 is confirmed by the pressure measurements from Chigier and Beér [13].

In both the converging nozzle and diverging cup, the term $(1 + C_F)^{-1}$ in Eq. (9) magnifies the respective increase and drop of swirl due to the change of the cross section area between the inlet and outlet. The difference between Eqs. (1) and (9) highlights the way changes of the swirl number are altered by pressure effects. Note that the conservation of axial momentum flux reported in Refs. [13] and [21] is interpreted here as C_F being small in Eq. (9).

Mechanical Energy Balance. The previous analysis is deepened on a more quantitative basis with the help of shape factors that are defined as follows. Axial and azimuthal velocities are first set dimensionless with shape factors that characterize the inhomogeneous nature of the considered velocity profiles. Let f_{zj} and $f_{\theta j}$, respectively, designate the dimensionless profiles of the axial and tangential velocities, with $j = 1, 2$

$$u_{zj}(r) = f_{zj}(r)U_{zj} \quad u_{\theta j}(r) = f_{\theta j}(r)U_{\theta j} \tag{10}$$

where U_{zj} and $U_{\theta j}$ are the area-averaged axial and tangential velocities shown in Fig. 8. They are defined as $U_{ij}A_j = \int_{A_j} u_{ij}(r)\mathrm{d}A$. The shape factor $f_{ij}(r)$ needs in turn to comply with $\int_{A_j} f_{ij}(r)\mathrm{d}A = A_j$, with $i = z, \theta$ and $j = 1, 2$.

One can express the pressure-less swirl variation through a change of the cross section area by

$$\frac{\widetilde{S}_2}{\widetilde{S}_1} = \frac{R_2}{R_1}\frac{\int_{A_1} f_{z1}^2(r)\mathrm{d}A/A_1}{\int_{A_2} f_{z2}^2(r)\mathrm{d}A/A_2} \tag{11}$$

Due to the angular momentum conservation, change of the swirl number is fully controlled by the axial flow velocity profile at the control volume boundaries. This expression generalizes Eq. (1) from Gupta and Lilley [4] established for a constant axial velocity ($f_{z1} = f_{z2} = 1$) to velocity profiles of arbitrary shapes obeying to Eq. (10).

Equation (11) is now used to highlight the impact of the structure of the velocity profiles on the evolution of the swirl number. The LDV measurements reported in Fig. 7 are used to determine the shape factors f_{z1} and f_{z2} at the diffuser outlet, for two different diffusers of respective radius R_1 and R_2. In doing so, one retrieves the experimental result $\widetilde{S}_2/\widetilde{S}_1 \simeq 1$, as in Eq. (4). Therefore, the use of shape factors in Eq. (11) reconciliates the evolution of the swirl number Eq. (4) measured by LDV with the model Eq. (1) from Gupta and Lilley. This validation underlines that the value of the swirl number mainly relies on the assumptions made on the velocity profiles.

Shape factors are now used to determine the dimensionless coefficient C_F in Eq. (9) by a balance of mechanical energy applied to the control volume delimited by the inlet A_1 and outlet A_2 sections of the diverging quarl. The flow is again considered as steady. The mechanical energy balance is expressed in its integral form

$$\int_{A_1} \left(\frac{1}{2}\rho \mathbf{v}^2 + p\right)\mathbf{v} \cdot \mathbf{n}\mathrm{d}A - \int_{A_2} \left(\frac{1}{2}\rho \mathbf{v}^2 + p\right)\mathbf{v} \cdot \mathbf{n}\mathrm{d}A = k\int_{A_1} \frac{1}{2}\rho u_z^2 \mathbf{v} \cdot \mathbf{n}\mathrm{d}A \tag{12}$$

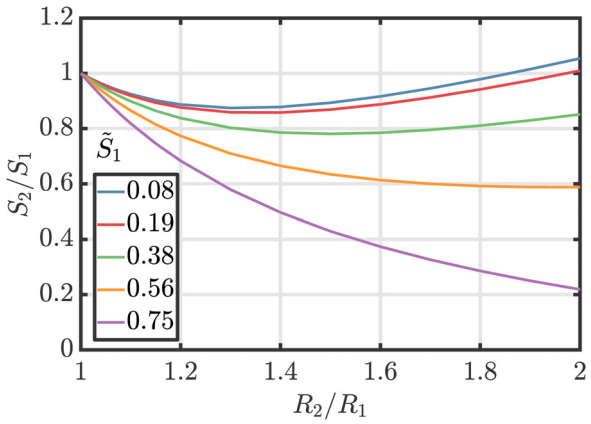

Fig. 9 Swirl number ratio S_2/S_1 for different inlet pressure-less swirl number S_1, with $k=0$

where k denotes the head loss through the diverging quarl. Mass, momentum, and energy balances are rewritten with the help of shape factors. Quantities are set dimensionless with respect to U_{z1}. For a fixed ratio $U_{\theta 1}/U_{z1}$ characterizing the angular velocity of the upstream flow, the set of three balance equations is solved to determine the ratios U_{z2}/U_{z1}, $U_{\theta 2}/U_{z2}$, and $(p_1-p_\infty)/(\rho U_{z1}^2)$. Once the shape functions $f_{zj}(r)$ and $f_{\theta j}(r)$ are fixed, the swirl number S_2/S_1 comes as a result.

An analytical solution is derived for a uniform axial flow $f_{zj}=1$ and a solid-body rotation $f_{\theta j}=(3/2)(r/R)$ at the inlet ($j=1$) and outlet ($j=2$) of the diffuser, as Gupta and Lilley [4] did in their model Eq. (1). The resolution of the system leads to

$$C_p=\frac{p_2-p_1}{\rho U_{z1}^2/2}=(1-x^{-2})\left(x^{-2}+1+2\widetilde{S_1}^2\right)-k \tag{13}$$

and

$$\frac{S_2}{S_1}=x\left[1+\frac{k}{2}+\frac{1}{2}(x^{-2}-1)\left(x^{-2}+1+2\widetilde{S_1}^2\right)\right] \tag{14}$$

where $x=R_2/R_1$ and $\widetilde{S}_1=(\Omega_1 R_1/2U_{z1})$ designates the pressure-less swirl number, and Ω_1 is the angular velocity at the diffuser inlet. It appears that the ratio of the swirl number does not only depend on the ratio R_2/R_1 but also on the pressure-less swirl number $\widetilde{S}_1$ and head loss k. As the swirl evolution is not straightforward in Eq. (14), a Taylor expansion in the neighborhood of $R_1=R_2$ yields

$$\frac{S_2}{S_1}=1+\frac{k}{2}-\left(\frac{R_2}{R_1}-1\right)\left(1+2\widetilde{S_1}^2-\frac{k}{2}\right) \tag{15}$$

This latter expression describes the decline of the swirl number through a small diverging cup.

Figure 9 depicts the swirl number evolution through a diffuser for different inlet swirl numbers S_1 in the absence of head loss $k=0$. The scope of these formula remains limited as the head loss k needs to be specified and depends itself on several flow parameters. It is, however, shown here that the pressure contribution to the swirl number can be evaluated with a balance of mechanical energy. This energy budget shows that an increasing swirl level $\widetilde{S}_1$ at the diffuser inlet leads to a higher kinetic energy loss through the diffuser, so that G_{z1} decreases with p_1-p_2, yielding a smaller ratio S_2/S_1.

As a conclusion, the impact of the quarl angle on the swirl number S has been analyzed: (i) through LDV measurements of the pressure-less swirl number $\widetilde{S}$, (ii) with a theoretical analysis of the swirl number S evolution with the help of Eq. (9), (iii) with the help of shape factors to solve the mechanical energy balance in Eq. (14). It has been shown that in all three cases, the swirl number decreases with the quarl angle expansion, and that the pressure-less swirl number $\widetilde{S}$ is not altered by smooth changes of the cross section area of the injector. This theoretical analysis confirms that changes of the swirl level S through the injector diffuser cup, regardless the method used to evaluate this change, cannot explain the structure of the flame and flow patterns observed in the experiments when the injector cup angle is varied.

It is at this point worth recalling the assumptions made in the analysis carried out in this work. First, the theoretical expressions Eqs. (9) and (14) result from inviscid theory, in which effects of turbulence have been neglected. Measurements of the swirl number carried out in this work do not include effects of the turbulent velocity fluctuations either. Second, as the overall study focuses on the influence of the quarl angle, all other geometrical parameters that are known to alter the flame and flow patterns have been kept constant. For instance, effects of the injector geometry have been investigated in Ref. [23]. Effects of the combustion chamber confinement have been investigated in Ref. [9], and this study pertains to situations in which the confinement ratio is large.

Impact of Quarl on the Stagnation Point Position of the Internal Recirculation Zone. Measurements in Fig. 4 show that the growth of the IRZ is promoted by a large increase of the radial velocity component of the flow when the quarl angle rises from 0 deg up to 45 deg. Through the continuity equation, the gradient of radial velocity is balanced with the negative gradient of axial velocity in the vicinity of the diverging nozzle outlet. The following analysis is carried out so as to provide a model for the displacement of the position of the IRZ toward the injector outlet when the quarl angle increases.

Let assume that a swirling jet passes through a diverging quarl, with a sufficiently high level of swirl to create an IRZ in the combustion chamber, as sketched in Fig. 10. Pressures, velocities, and cross section areas are indexed by 1 at the diffuser inlet, and by 2 at the outlet of the diverging cup. The quarl outlet also defines the axial origin, whereas z_{SP} stands for the axial coordinate of the stagnation point defining the lower position of the IRZ along the burner axis.

The axial velocity gradient along the burner axis is set by the adverse pressure gradient, no matter the swirl motion

$$\frac{\partial p}{\partial z}=-\rho u_z\frac{\partial u_z}{\partial z} \tag{16}$$

The adverse pressure gradient is promoted by the expansion of the quarl and stays positive up to the stagnation point z_{SP}. The momentum balance Eq. (16) is now evaluated at the quarl outlet $z=0$. Figure 5 indicates that the swirling jet opening angle β regularly increases like the angle α of the diffuser cup as long as it lies in the free jet regime: $\beta\simeq\alpha$ when $\alpha<30$ deg. Therefore, following the streamlines, the pressure gradient at the quarl outlet in section (2) is then equal to the pressure gradient at the quarl inlet in section (1)

$$\frac{p_2-p_1}{h}\sim-\rho u_{z2}\frac{\partial u_z}{\partial z}\bigg|_{z=0} \tag{17}$$

The impact of the IRZ on the flow in the vicinity of the injector outlet can be modeled as a stagnation flow with a strain rate ε. The inviscid flow thus obeys to $u_z=u_{z2}-\varepsilon z$, and $z_{SP}=u_{z2}/\varepsilon$. By eliminating ε, the height of the stagnation point thus scales as

$$\frac{z_{SP}}{h}\sim\left(\frac{A_1}{A_2}\right)^2\frac{1}{C_p}\quad\text{with}\quad C_p=\frac{p_2-p_1}{\rho U_{z1}^2} \tag{18}$$

The pressure coefficient C_p is given by Eq. (13) showing that a diverging quarl increases the pressure drop C_p positively.

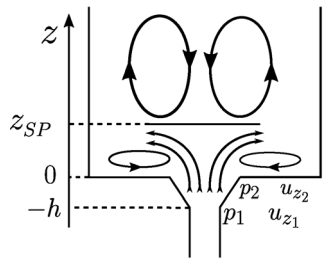

Fig. 10 Schematic of the swirled flow pattern depicted as a stagnation flow between the injector quarl and the IRZ

Equation (18) states that the adverse pressure gradient moves the stagnation point z_{SP} further upstream closer to the injector outlet due to the cross section area ratio $(A_1/A_2)^2$ and the inverse of the pressure coefficient $1/C_p$ that both decrease for increasing quarl angles.

This behavior is precisely the one which is observed in Figs. 4 and 5. Predictions from Eq. (18) are superimposed to the measurements of the IZR leading edge position along the burner axis in Fig. 5. To do so, the values found for $\widetilde{S} = 0.85$ and $k = 0.5$ are used to determine C_p with Eq. (13), and the model is calibrated with the measurements made for $\alpha = 10$ deg. No difference has been found when changing the head loss coefficient from $k = 0$ up to $k = 1$ because the major contribution in Eq. (18) lies in the area ratio A_1/A_2. The match between the model and the measurements is excellent in Fig. 5, except in the absence of quarl when $\alpha = 0$ deg. In this case, the adverse pressure gradient in Eq. (16) is not related to the quarl, but to the natural expansion of the swirling jet, a feature which is not taken into account in the present analysis.

It has been shown that the position of the leading edge front of a swirling flame can be controlled in the Oxytec test-rig by adjusting the angle of the diffuser cup from the injector. It has then been demonstrated that the resulting modification of the swirl level due to the quarl does not take part in the process because the diverging cup reduces the swirl number S as seen in Eq. (4) and let the pressure-less swirl number $\widetilde{S}$ unaltered (Eq. (9)) in the Oxytec test-rig. It has then been shown that the axial velocity gradient at the injector outlet mainly depends on both the magnitude of the axial velocity and the pressure drop induced by the quarl. Expanding the quarl leads to a stronger adverse pressure gradient and a reduction of the axial flow velocity.

Though assuming a stagnation flow pattern at the burner outlet constitutes a rough approximation of reality, the model Eq. (17) developed in this study successfully reproduces the evolution of the stagnation point position z_{SP} of the internal recirculation region as a function of the axial velocity gradient at the burner outlet $\partial u_z/\partial z(z = 0)$ as observed in the experiments. This physics based model may be used as a starting point to develop more realistic representations of the swirled flow at the outlet of a swirling injector and needs to be further corroborated with other injector technologies.

Conclusion

The impact of a diverging cup on the structure of technically premixed swirling flames has been investigated experimentally and theoretically. In this study, flames are stabilized aerodynamically at the injector outlet of the flow produced by an axial-plus-tangential swirler ended by a diffuser cup with an adjustable angle.

Flame topologies have been observed with OH* chemiluminescence imaging. These visualizations completed by particle image velocimetry and OH laser-induced fluorescence measurements in reacting conditions have provided information on the structure of the flame and the internal recirculation zone produced by the injector with different diffusers. For a given geometrical swirl number calculated before the diffuser cup, increasing the quarl angle considerably widens the central recirculation region, shortens the flame, and moves the position of the central recirculation bubble further upstream closer to the burner outlet. A large value of the quarl angle can place the flow and flame patterns in the wall-jet regime, at a confinement ratio where a free-jet regime is generally produced in the absence of quarl.

Measurements in nonreacting flow conditions revealed a very similar evolution of the position of the internal recirculation region as the quarl angle widens with results obtained under reacting conditions. Laser Doppler velocimetry measurements have been carried out to determine the swirl number without pressure terms for the different quarl angles tested. It has been found that the pressure-less swirl number $\widetilde{S}$ remains unaltered despite the quarl expansion, a result which conflicts with the predictions from Gupta and Lilley [4]. The measured swirl levels $\widetilde{S}$ are therefore seen not to account for the drastic increase of the size of the internal recirculation bubble as the quarl angle increases.

A theoretical analysis has been carried out to take the pressure contribution into account in the swirl number S and examine the impact of a diverging cup on the swirl number evolution. It has been found that the swirl number S decreases as the quarl angle increases, and that this trend is magnified when pressure effects are included. The pressure contribution reduces the upstream axial momentum flux. Hence, neither the measured pressure-less swirl number nor the theoretical estimates allow to account for the flame and flow patterns observed in the experiments. It is firmly concluded that the swirl number is not the relevant dimensionless quantity to assess the impact of a nozzle cup on the flow patterns and stabilization of swirling flames when the quarl angle is varied, all other parameters remaining fixed.

It has finally been shown that the decrease of the axial flow velocity and increase of the adverse pressure gradient at the burner outlet are both responsible for the displacement of the position of the stagnation point of the internal recirculation zone as the quarl angle increases. Expansion of the cross section of the diffuser leads to a reduction of the axial momentum flux per unit area, which reduces the jet ability to push the internal recirculation zone further downstream. A theoretical model has been developed that well reproduces the experimental data for the diffuser cup angles tested between $5\,\text{deg} \leq \alpha \leq 30\,\text{deg}$ by assuming that the swirling flow takes the structure of a stagnation flow at the burner outlet.

Acknowledgment

This work is supported by the Air Liquide, CentraleSupélec and CNRS Chair on oxy-combustion and heat transfer for energy and environment and by the OXYTEC project (ANR-12-CHIN-0001) from lrom)12- Nationale de la Recherche. The authors are grateful to the technical staff of EM2C for their assistance during the design and construction of the experimental setup.

Funding Data

- Agence Nationale de la Recherche (ANR-12-CHIN-0001).

References

[1] Rawe, R., and Kremer, H., 1981, "Stability Limits of Natural Gas Diffusion Flames With Swirl," Symp. (Int.) Combust., **18**(1), pp. 667–677.
[2] Syred, N., 2006, "A Review of Oscillation Mechanisms and the Role of the Precessing Vortex Core (PVC) in Swirl Combustion Systems," Prog. Energy Combust. Sci., **32**(2), pp. 93–161.
[3] Beér, J. M., and Chigier, N. A., 1972, *Combustion Aerodynamics*, Applied Science/Halsted-Wiley, London/New York.
[4] Gupta, A. K., Lilley, D. G., and Syred, N., 1984, *Swirl Flows*, Abacus Press, Tunbridge Wells, Kent, UK.
[5] Cheng, R., Yegian, D., Miyasato, M., Samuelsen, G., Benson, C., Pellizzari, R., and Loftus, P., 2000, "Scaling and Development of Low-Swirl Burners for Low-Emission Furnaces and Boilers," Proc. Combust. Inst., **28**(1), pp. 1305–1313.

[6] Chterev, I., Sundararajan, G., Seitzman, J., and Lieuwen, T., 2015, "Precession Effects on the Relationship Between Time-Averaged and Instantaneous Swirl Flow and Flame Characteristics," ASME Paper No. GT2015-42768.

[7] Burmberger, S., Hirsch, C., and Sattelmayer, T., 2006, "Designing a Radial Swirler Vortex Breakdown Burner," ASME Paper No. GT2006-90497.

[8] Toh, K., Honnery, D., and Soria, J., 2010, "Axial plus Tangential Entry Swirling Jet," Exp. Fluids, **48**(2), pp. 309–325.

[9] Fanaca, D., Alemela, P., Hirsch, C., and Sattelmayer, T., 2010, "Comparison of the Flow Field of a Swirl Stabilized Premixed Burner in an Annular and a Single Burner Combustion Chamber," ASME J. Eng. Gas Turbines Power, **132**(7), p. 071502.

[10] Mongia, H., 2011, "Engineering Aspects of Complex Gas Turbine Combustion Mixers—Part III: 30 OPR," AIAA Paper No. 2011-5525.

[11] Chong, L. T. W., Komarek, T., Zellhuber, M., Lenz, J., Hirsch, C., and Polifke, W., 2016, "Combined Influence of Strain and Heat Loss on Turbulent Premixed Flame Stabilization," Flow, Turbulence and Combust., **97**, pp. 263–294.

[12] Guiberti, T., Durox, D., Scouflaire, P., and Schuller, T., 2015, "Impact of Heat Loss and Hydrogen Enrichment on the Shape of Confined Swirling Flames," Proc. Combust. Inst., **35**(2), pp. 1385–1392.

[13] Chigier, N. A., and Beér, J. M., 1964, "Velocity and Static-Pressure Distributions in Swirling Air Jets Issuing From Annular and Divergent Nozzles," J. Basic Eng., **86**(4), pp. 788–796.

[14] Terhaar, S., Oberleithner, K., and Paschereit, C. O., 2014, "Impact of Steam-Dilution on the Flame Shape and Coherent Structures in Swirl-Stabilized Combustors," Combust. Sci. Technol., **186**(7), pp. 889–911.

[15] Vanoverberghe, K. P., Bulck, E. V. V. D., and Tummers, M. J., 2003, "Confined Annular Swirling Jet Combustion," Combust. Sci. Technol., **175**(3), pp. 545–578.

[16] Therkelsen, P. L., Littlejohn, D., Cheng, R. K., Portillo, J. E., and Martin, S. M., 2010, "Effect of Combustor Inlet Geometry on Acoustic Signature and Flow Field Behavior of the Low Swirl Injector," ASME Paper No. GT2010-23498.

[17] Jourdaine, P., Mirat, C., Beaunier, J., Caudal, J., Joumani, Y., and Schuller, T., 2016, "Effect of Quarl on N_2- and CO_2-Diluted Methane Oxy-Flames Stabilized by an Axial-plus-Tangential Swirler," ASME Paper No. GT2016-56953.

[18] Weber, R., and Dugué, J., 1992, "Combustion Accelerated Swirling Flows in High Confinements," Prog. Energy Combust. Sci., **18**(4), pp. 349–367.

[19] Syred, N., and Bekr, J. M., 1974, "Combustion in Swirling Flows: A Review," Combust. Flame, **201**(2), pp. 143–201.

[20] Mattingly, J. D., Oates, G. C., Dolling, D. S., and Gray, W. K., 1986, "An Experimental Investigation of the Mixing of Coannular Swirling Flows," AIAA J., **24**(5), pp. 785–792.

[21] Mahmud, T., Truelove, J. S., and Wall, T. F., 1987, "Flow Characteristics of Swirling Coaxial Jets From Divergent Nozzles," ASME J. Fluids Eng., **109**(3), pp. 275–282.

[22] Jourdaine, P., Mirat, C., Caudal, J., Lo, A., and Schuller, T., 2017, "A Comparison Between the Stabilization of Premixed Swirling CO_2-Diluted Methane Oxy-Flames and Methane/Air Flames," Fuel, **201**, pp. 156–164.

[23] Jourdaine, P., Mirat, C., Caudal, J., and Schuller, T., 2017, "Stabilization Mechanisms of Swirling Premixed Flames With an Axial-Plus-Tangential Swirler," ASME J. Eng. Gas Turbines Power **140**(8), p. 081502.

[24] Guiberti, T. F., Durox, D., Zimmer, L., and Schuller, T., 2015, "Analysis of Topology Transitions of Swirl Flames Interacting With the Combustor Side Wall," Combust. Flame, **162**(11), pp. 4342–4357.

[25] Lefebvre, A. H., 2010, *Gas Turbine Combustion: Alternative Fuels and Emissions*, CRC Press, Boca Raton, FL.

[26] Jourdaine, P., 2017, "Analyse des mécanismes de stabilisation d'oxy-flammes prémélangées swirlées," Doctoral dissertation, CentraleSupélec, Université Paris Saclay, France.

[27] Reichel, T. G., Terhaar, S., and Paschereit, O., 2015, "Increasing Flashback Resistance in Lean Premixed Swirl-Stabilized Hydrogen Combustion by Axial Air Injection," ASME J. Eng. Gas Turbines Power, **137**(7), p. 071503.

[28] Schlichting, H., Gersten, K., Krause, E., and Oertel, H., 1955, *Boundary-Layer Theory*, Vol. 7, Springer, Berlin.